

Article

Defect-Induced π -Magnetism into Non-Benzenoid Nanographenes

Kalyan Biswas ^{1,†}, Lin Yang ^{2,†}, Ji Ma ^{2,*}, Ana Sánchez-Grande ¹, Qifan Chen ³, Koen Lauwaet ¹, José M. Gallego ⁴, Rodolfo Miranda ^{1,5}, David Ěcija ^{1,*}, Pavel Jelínek ^{3,6,*}, Xinliang Feng ² and José I. Urgel ^{1,*} 

- ¹ IMDEA Nanoscience, C/Faraday 9, Campus de Cantoblanco, 28049 Madrid, Spain; kalyan.biswas@imdea.org (K.B.); ana.sanchez@imdea.org (A.S.-G.); koen.lauwaet@imdea.org (K.L.); rodolfo.miranda@imdea.org (R.M.)
- ² Center for Advancing Electronics, Faculty of Chemistry and Food Chemistry, Technical University of Dresden, 01062 Dresden, Germany; Lin.Yang1@tu-dresden.de (L.Y.); Xinliang.Feng@tu-dresden.de (X.F.)
- ³ Institute of Physics of the Czech Academy of Science, CZ-16253 Praha, Czech Republic; chenq@fzu.cz
- ⁴ Instituto de Ciencia de Materiales de Madrid, CSIC, Cantoblanco, 28049 Madrid, Spain; josemaria.gallego@imdea.org
- ⁵ Departamento de Física de la Materia Condensada, Universidad Autónoma de Madrid, 28049 Madrid, Spain
- ⁶ Regional Centre of Advanced Technologies and Materials, Palacký University Olomouc, CZ-77146 Olomouc, Czech Republic
- * Correspondence: ji.ma@tu-dresden.de (J.M.); david.ecija@imdea.org (D.Ě.); jelinekp@fzu.cz (P.J.); jose-ignacio.urgel@imdea.org (J.I.U.)
- † These authors contributed equally to this work.

Abstract: The synthesis of nanographenes (NGs) with open-shell ground states have recently attained increasing attention in view of their interesting physicochemical properties and great prospects in manifold applications as suitable materials within the rising field of carbon-based magnetism. A potential route to induce magnetism in NGs is the introduction of structural defects, for instance non-benzenoid rings, in their honeycomb lattice. Here, we report the on-surface synthesis of three open-shell non-benzenoid NGs (**A**₁, **A**₂ and **A**₃) on the Au(111) surface. **A**₁ and **A**₂ contain two five- and one seven-membered rings within their benzenoid backbone, while **A**₃ incorporates one five-membered ring. Their structures and electronic properties have been investigated by means of scanning tunneling microscopy, noncontact atomic force microscopy and scanning tunneling spectroscopy complemented with theoretical calculations. Our results provide access to open-shell NGs with a combination of non-benzenoid topologies previously precluded by conventional synthetic procedures.

Keywords: on-surface synthesis; nanomagnetism; polycyclic aromatic hydrocarbons; nanographenes; open-shell character; STM; nc-AFM



Citation: Biswas, K.; Yang, L.; Ma, J.; Sánchez-Grande, A.; Chen, Q.; Lauwaet, K.; Gallego, J.M.; Miranda, R.; Ěcija, D.; Jelínek, P.; et al. Defect-Induced π -Magnetism into Non-Benzenoid Nanographenes. *Nanomaterials* **2022**, *12*, 224. <https://doi.org/10.3390/nano12020224>

Academic Editor:
Carlos Sanchez-Sanchez

Received: 16 December 2021

Accepted: 6 January 2022

Published: 11 January 2022

Publisher's Note: MDPI stays neutral with regard to jurisdictional claims in published maps and institutional affiliations.



Copyright: © 2022 by the authors. Licensee MDPI, Basel, Switzerland. This article is an open access article distributed under the terms and conditions of the Creative Commons Attribution (CC BY) license (<https://creativecommons.org/licenses/by/4.0/>).

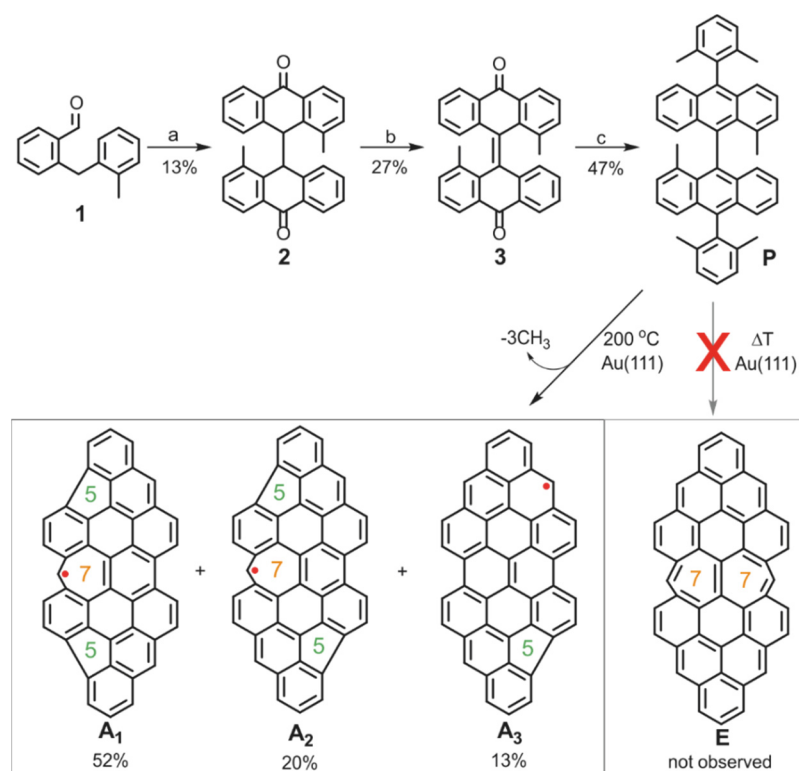
1. Introduction

The physicochemical properties of well-defined compounds that consist of fused conjugated aromatic rings, frequently referred as to polycyclic aromatic hydrocarbons or NGs [1], have been under the spotlight over the last years due to their potential in great number of technological applications [2–4]. Tuning such properties is feasible by modifying some of their structural characteristics as: (i) size, (ii) edge topology [5,6] or (iii) by introducing structural defects in the honeycomb lattice [7,8]. While the majority of NGs, known to be model compounds in organic chemistry, accommodates π -electrons in the bonding orbitals conferring them a closed-shell singlet ground state; compounds comprising unpaired or partially unpaired electrons within the molecular backbone, i.e., with an open-shell ground state, display unique electronic properties capable of carrying magnetism and conductivity functionalities [9–12]. However, their high reactivity usually

makes conventional solution-mediated synthesis of open-shell NGs a great challenge, limiting the number of available compounds.

The synthesis of novel reactive compounds confined on a metallic surface under ultra-high vacuum (UHV) conditions has emerged as a compelling alternative synthetic toolbox toward the design of open-shell NGs [13]. For instance, the nature of the electronic ground state of long pursued members of the acene [14–19] and triangulene [20,21] families, widely discussed in theoretical studies, have only recently been untangled. Contemporarily, a successful strategy toward the on-surface formation of open-shell NGs, one-dimensional polymers and graphene nanoribbons (GNRs) is the surface-assisted oxidative ring closure between a methyl group and the neighboring aryl moiety of a properly predesigned molecular precursor, which occurs after thermal activation [22–37]. Such synthetic approach, though often successful, presents some limitations related to the cleavage of methyl groups prior to cyclization, which may lead to the formation of topological defects inducing an open-shell ground state to NGs [30,37].

In this article, we report the synthesis of three open-shell non-benzenoid NGs (A_1 , A_2 and A_3) with a total spin (S) = 1/2 in their atomic lattice, resulting from the on-surface reactions of the 10,10'-bis(2,6-dimethylphenyl)-1,1'-dimethyl-9,9'-bianthracene precursor (P) on Au(111) in a UHV environment (Scheme 1). Our attempts to synthesize the expected heptalene-embedded NG (E) on the gold surface were ineffective due to the propensity of methyl groups to cleave prior to oxidative ring closure. The chemical structure of the three NGs is clearly determined by scanning tunneling microscopy (STM) and noncontact atomic force microscopy (nc-AFM). Moreover, their electronic properties are studied by scanning tunneling spectroscopy (STS) and complemented by density functional theory (DFT) calculations, which indicates the presence of an unpaired spin detected as a Kondo resonance.



Scheme 1. Conceptual routes toward the formation of open-shell non-benzenoid NGs on Au(111). Reagents and conditions: (a) $K_2S_2O_8$, tetraethylammonium bromide, 1,2-dichloroethane, 120 °C, 36 h. (b) (i) KOH, EtOH, reflux, 0.5 h; (ii) $K_2S_2O_8$, H_2O , rt., 2 h. (c) (i) 2,6-dimethylphenylmagnesium bromide, THF, 0 °C-rt., 24 h; (ii) NaI, $NaH_2PO_2 \cdot H_2O$, CH_3COOH , reflux, 2 h.

2. Experimental Details

Experiments were performed in a custom-designed ultra-high vacuum system (base pressure below 4×10^{-10} mbar) hosting a commercial low-temperature microscope with STM/AFM capabilities from Scienta Omicron and located at IMDEA Nanoscience (Madrid, Spain).

The Au(111) substrate was prepared by repeated cycles of Ar⁺ sputtering ($E = 1.5$ keV) and subsequent annealing at 740 K for 10 min. All STM images shown were taken in constant-current mode, unless otherwise noted, with electrochemically etched tungsten tips, at a sample temperature of 4.3 K (LakeShore, Carson, CA, USA). Scanning parameters are specified in each figure caption. The molecular precursor was thermally deposited (Kentax TCE-BSC, Seelze, Germany) onto the clean Au(111) surface held at room temperature with a typical deposition rate of 0.5 Å/min (sublimation temperature of 170 °C), controlled by a quartz micro balance (LewVac, Burgess hill, United Kingdom). After deposition of P, the sample was post-annealed at 200 °C for 10 min to induce the cyclodehydrogenation reaction.

Non-contact AFM measurements were performed with a tungsten tip attached to a Qplus tuning fork sensor (Omicron, Taunusstein, Germany) [38]. The tip was functionalized a posteriori by the controlled adsorption of a single CO molecule at the tip apex from a previously CO-dosed surface [39]. The functionalized tip enables the imaging of the intramolecular structure of organic molecules [40]. The sensor was driven at its resonance frequency (~26 kHz for Qplus) with a constant amplitude of ~80 pm. The shift in the resonance frequency of the sensor (with the attached CO-functionalized tip) was recorded in a constant-height mode (Omicron Matrix electronics and MFLi PLL by Zurich Instruments (Zurich, Switzerland) for Omicron). The STM and nc-AFM images were analyzed using WSxM 5.0 (Madrid, Spain) [41].

3. Results and Discussion

3.1. On-Surface Synthesis of Non-Benzenoid Nanographenes

Since the synthesis of E through conventional solution synthesis methods was unsuccessful, we directed our attention to the on-surface synthesis approach. Thus, a first step toward the formation of a heptalene-embedded non-benzenoid nanographene involves the synthesis of the molecular precursor P, which was prepared by solution chemistry. As shown in Scheme 1, compound 2 was firstly obtained by the oxidative acylation reaction and homo-coupling of 2-(2-methylbenzyl)benzaldehyde 1, which was then enolized and dehydrogenated to yield the bisanthrone derivative 3. After that, derivative 3 was treated with 2,6-dimethylphenylmagnesium bromide, followed by reduction to afford 10,10'-bis(2,6-dimethylphenyl)-1,1'-dimethyl-9,9'-bianthracene precursor (P). The six methyl groups from P are expected to undergo surface-catalyzed oxidative ring closure, and the final compound E is expected to comprise two triangulene subunits connected by two heptagons. With this aim, a low coverage of P (0.1 ML) was deposited onto an Au(111) surface held at room temperature. Subsequent annealing of the sample at 200 °C affords the formation of distinct non-benzenoid NGs coexisting with some fused nanostructures, as observed in the STM images shown in Figure 1a,b. The formation of such NGs is attributed to the oxidative ring closure of the majority of the methyl groups, together with the dissociation of several of them per NG prior to cyclization. Such removal of methyl moieties was previously reported in the synthesis of several NGs [30,37,42–45] and GNRs [22,46] and is concomitant to the annealing step at temperatures where the oxidative ring closure is expected to occur on Au(111), therefore being not possible to achieve the synthesis of E.

In order to obtain further structural information of the formed NGs, constant-height frequency-shift nc-AFM measurements acquired using a CO-terminated tip were performed [40,47]. The majority (~85%) of the formed NGs (A₁–A₃) are shown in Figure 1c–e. All of them feature a planar conformation on the surface. The images depicting A₁ (Figure 1c) and A₂ (Figure 1d) allow us to discern the formation of two five- and one six-membered rings, attributed to the loss of three methyls (green and blue arrows, respectively), together with the expected formation of one seven-membered ring (orange arrows) and two six-membered rings via oxidative ring closure (red arrows). The main structural

difference between both NGs is the location of one of the formed five-membered rings, depending on which methyl detached prior to oxidative ring closure from the (dimethyl) phenyl subunits. Similarly, A_3 (Figure 1e) arises from the loss of three methyls, giving rise to the formation of one five- and two six-membered rings (green and blue arrows, respectively), together with the expected formation of three six-membered rings (red arrows). In addition, a minority of benzenoid NGs [36], together with methyl migration and some fused species were observed on the Au(111) surface (see Figure S1 for their structural characterization). Therefore, A_1 – A_3 incorporate odd-membered rings at different positions of their atomic lattice in which a non-Kekulé structure is expected with a total spin $S = \frac{1}{2}$, as shown in the chemical sketches in Figure 1c–e [10,29,48–50].

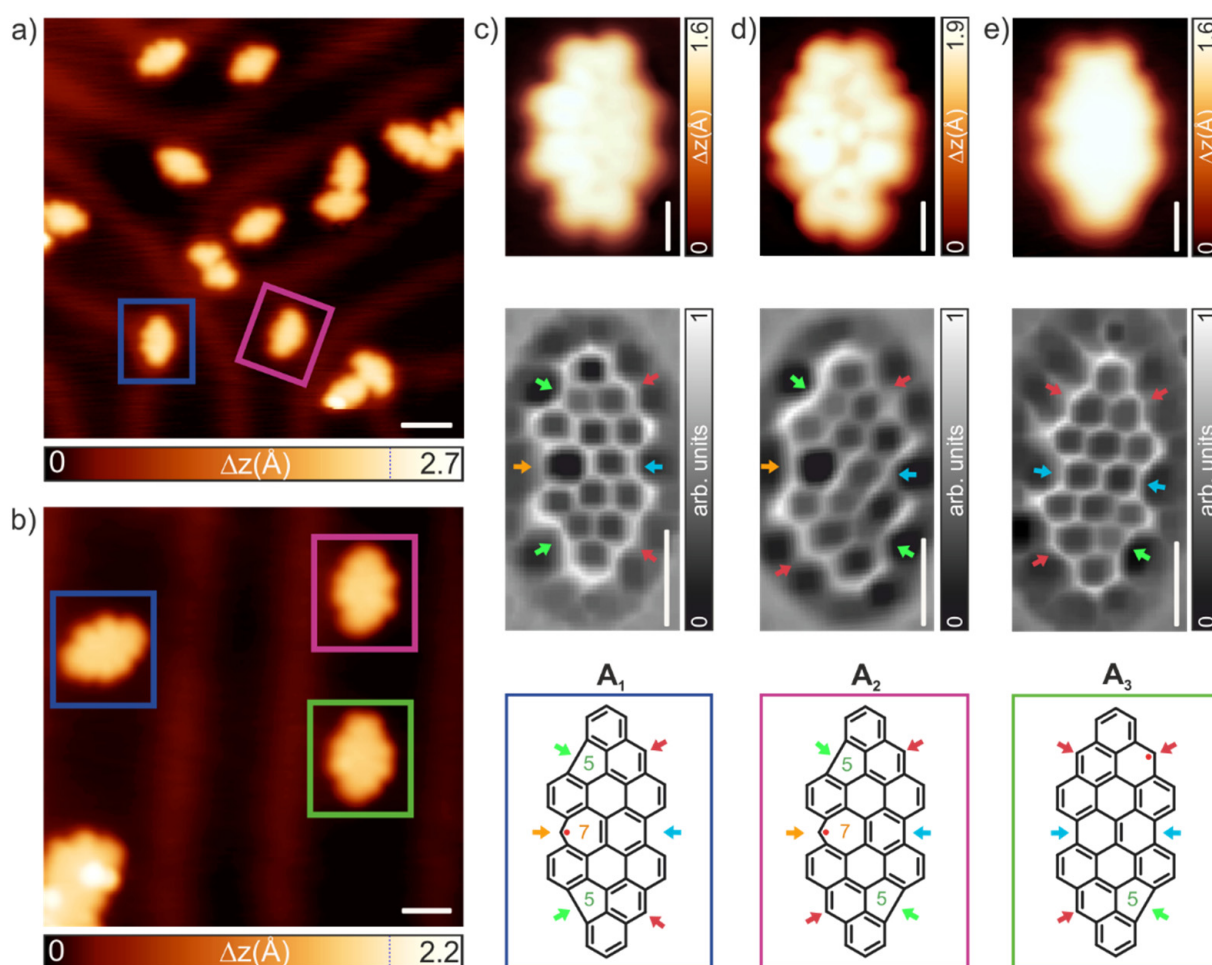


Figure 1. Synthesis and structural characterization of non-benzenoid NGs on Au(111). (a,b) Overview STM images of the Au(111) surface after sublimation of **P** and subsequent annealing at 200 °C. Scanning parameters: (a) $V_b = -1.5$ V, $I_t = 10$ pA and (b) $V_b = -1.5$ V, $I_t = 100$ pA. (a,b) Scale bars = 2 and 1 nm, respectively. (c–e) High-resolution STM images (top row) and constant-height frequency-shift nc-AFM (middle row) acquired with a CO-functionalized tip, together with the corresponding non-benzenoid non-Kekulé chemical structure (bottom row) of A_1 (c), A_2 (d) and A_3 (e). The colored rectangles of the distinct NGs correspond to the colored ones in (a,b) (blue (A_1), violet (A_2), and green (A_3)). The colored arrows highlight the formation of new rings as described in the main text. STM parameters: $V_b = 5$ mV, $I_t = 30$ pA, all scale bars = 0.5 nm. Nc-AFM parameters: Z offset = 150 pm above the STM set point (5 mV, 50 pA), scale bars = 1 nm.

3.2. Electronic and Magnetic Characterization of Non-Benzenoid Nanographenes

Next, we have inspected the electronic structure of the different non-benzenoid NGs (Figure 2a–c) via STS. The long-range differential conductance dI/dV spectra acquired on

A_1 – A_3 NGs show prominent resonances in the local density of states at around -0.9 V and $+1.4$ V for A_1 , -0.9 V and $+1.0$ V for A_2 , -1.0 V and $+1.4$ V for A_3 (Figure 2b). By acquiring dI/dV maps at those specific bias voltages and comparing them to the calculated dI/dV maps [47,51], such resonances are assigned to HOMO $- 1$ (HOMO = highest occupied molecular orbital) and LUMO $+ 1$ (LUMO = lowest unoccupied molecular orbital), respectively, as illustrated in Figure 2c. In addition, the trend in the energy gap between HOMO $- 1$ and LUMO $+ 1$ for A_1 – A_3 is in agreement with the one displayed by DFT calculations [52,53] of the free-standing NGs (see Figure S2), which altogether corroborates our rationalization of the electronic structure of the non-benzenoid species under study.

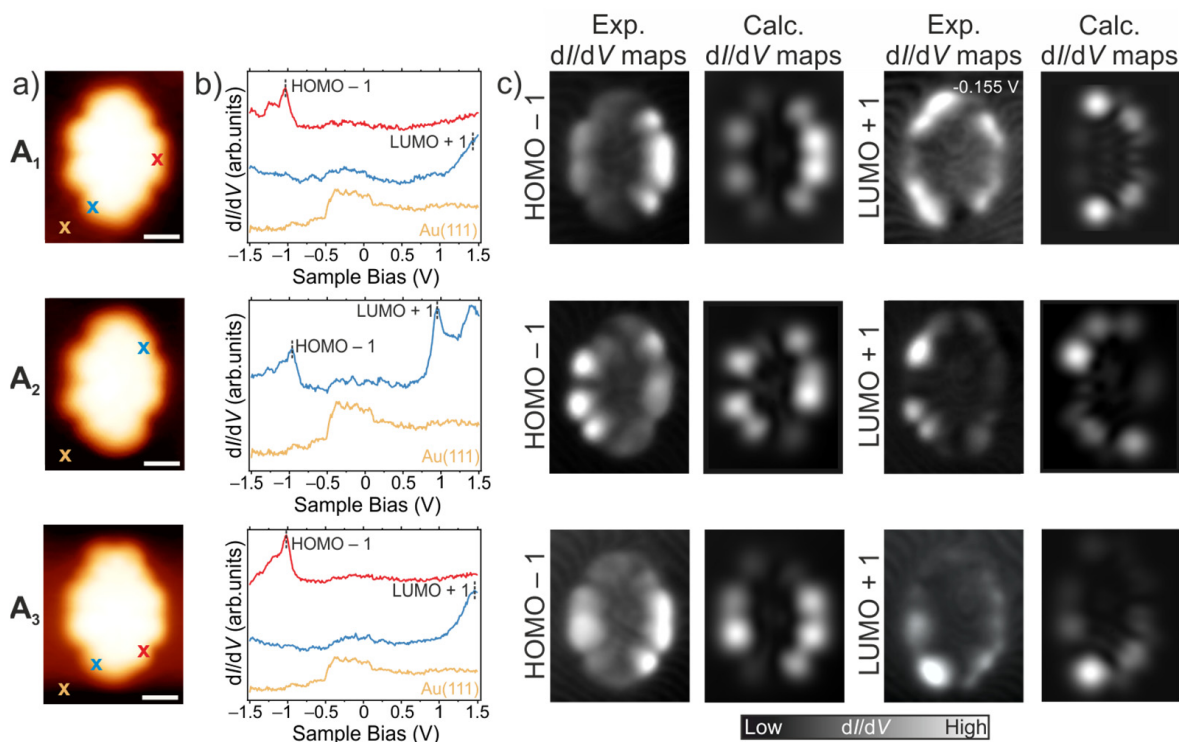


Figure 2. Electronic characterization of A_1 – A_3 on Au(111). (a) High-resolution STM images acquired with a CO-functionalized tip displaying the NGs marked with colored squares in (a). Scanning parameters: $V_b = -1.5$ V, $I_t = 100$ pA, all scale bars = 0.5 nm. (b) dI/dV spectra of A_1 – A_3 acquired at the positions indicated by the blue and red crosses in (b). Reference spectra taken on the bare Au(111) surface is depicted in orange and the acquisition positions marked with an orange cross. Open feedback parameters for dI/dV spectra: $V_b = -1.5$ V, $I_t = 250$ pA, $V_{rms} = 10$ mV. (c) Constant-current differential conductance (dI/dV) maps and corresponding DFT-calculated maps acquired with a CO-tip of the free-standing NGs (tip-sample height = 5 Å) at the energetic positions corresponding to the HOMO $- 1$ (left) and the LUMO $+ 1$ (right). Scanning parameters: A_1 : $V_b = -980$ mV, $I_t = 300$ pA (HOMO $- 1$), $V_b = 1400$ mV, $I_t = 300$ pA (LUMO $+ 1$). A_2 : $V_b = -980$ mV, $I_t = 250$ pA (HOMO $- 1$), $V_b = 880$ mV, $I_t = 250$ pA (LUMO $+ 1$). A_3 : $V_b = -980$ mV, $I_t = 300$ pA (HOMO $- 1$), $V_b = 1400$ mV, $I_t = 300$ pA (LUMO $+ 1$).

The open-shell non-Kekulé structures depicted in Figure 1c–e suggest that A_1 – A_3 should present an unpaired spin ($S = \frac{1}{2}$) per NG, having thus an open-shell ground state by definition [11]. Systems presenting an unpaired spin on a metallic substrate are typically expected to exhibit a Kondo resonance [54]. In order to demonstrate the singlet open-shell character of A_1 – A_3 , we have recorded dI/dV spectra at low bias voltages to observe any magnetic fingerprint. Interestingly, Figure 3a,c show pronounced low-bias peaks centered around the Fermi energy which are assigned to Kondo resonances, and can be nicely fitted by a Frota function, as expected for the Kondo phenomenon [55]. The determined half

width half maxima (HWHM) are 4.4 mV and 5.7 mV, indicating a Kondo temperature of 23 K and 47 K for A_1 and A_3 , respectively. Figure 3b shows a spectrum in the same bias range measured on A_2 . Again, a feature at low bias voltages is observed, but it is noticeably broader (HWHM of 15.4 mV), and has a slight offset toward positive bias values, centered at 3.3 mV. We tentatively attribute this feature to the orbital holding the unpaired spin, which is now above the Fermi level due to charge transfer with the underlying substrate. While long-range dI/dV spectroscopy on A_1 – A_3 provides clear evidence of the non-frontier states (HOMO – 1 and LUMO + 1), no explicit signatures of the frontier states (SOMOs = singly occupied molecular orbitals and SUMOs = singly unoccupied molecular orbitals) were observed [33,56]. However, constant-height STM images recorded close to the Fermi level resemble the shape of the calculated SOMO and SUMO (see Figure 3d–f), which corroborates the open-shell character of the studied NGs.

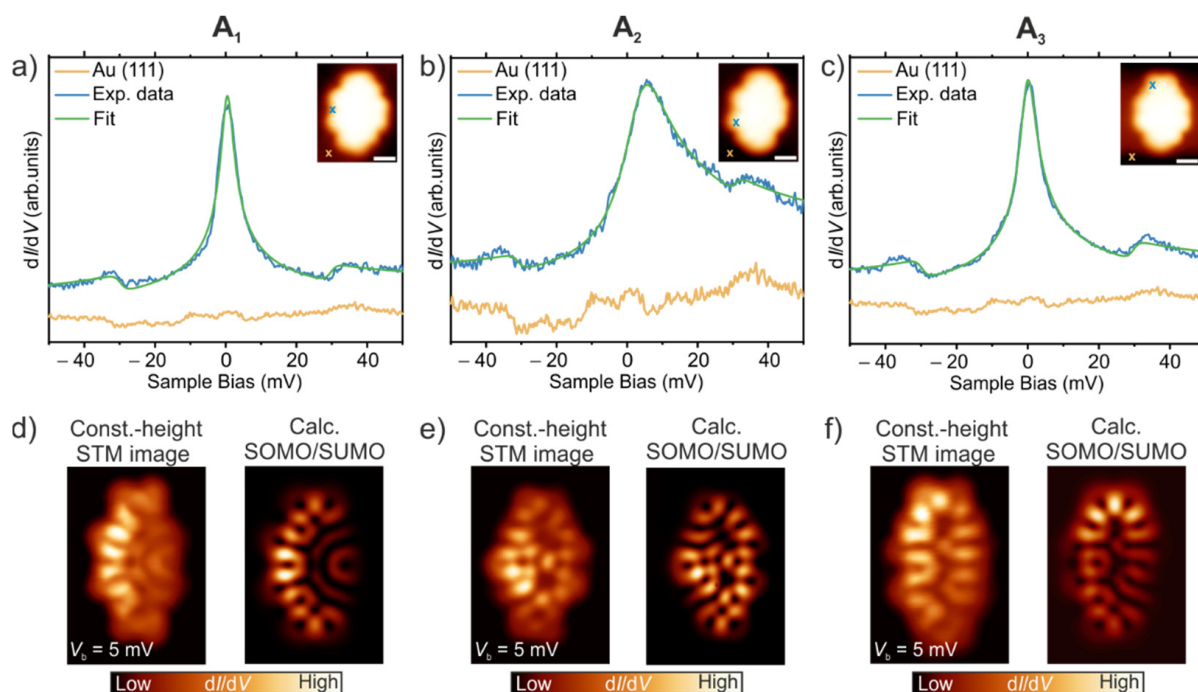


Figure 3. Open-shell character of A_1 – A_3 . (a–c) Short-range dI/dV spectra acquired at specific locations of A_1 – A_3 . The blue curves display the experimental data, and the green curves the corresponding Frota function fit. Orange curves depict the reference dI/dV spectra acquired on Au(111). Open feedback parameters: $V_b = -50$ mV, $I_t = 450$ pA, $V_{rms} = 2$ mV. (d–f) Constant-height STM images acquired at low bias voltages ($V_b = 5$ mV, $I_t = 30$ pA) and their comparison with the corresponding DFT-calculated maps of the SOMO/SUMO.

4. Conclusions

In conclusion, we have demonstrated the on-surface synthesis of well-defined open-shell non-benzenoid NGs (A_1 – A_3) on Au(111), via on-surface oxidative ring closure and methyl detachment of the parent precursor **P** upon annealing at 200 °C; and their structures have been clearly elucidated by STM and nc-AFM. Two of such NGs present one seven- and two five-membered rings (A_1 and A_2), while the last species features one five-membered ring (A_3). Importantly, the presence of such non-benzenoid rings render A_1 – A_3 as non-Kekulé structures which are expected to host an unpaired electron ($S = \frac{1}{2}$) per NG. STS studies, together with theoretical calculations, confirm the existence of such unpaired electron in two of the three species (A_1 and A_3) through the measurement of a Kondo resonance on the NGs. A_2 on the other hand, also presents a feature above the Fermi level, but in this case such resonance is attributed to the partial filling of the SOMO orbital, due to charge transfer with the underlying surface. The synthesized NGs can serve as model structures that help to understand the introduction of odd-member rings in the honeycomb

lattice of graphene nanostructures, paving avenues to engineer novel non-benzenoid NGs on surfaces of interest in molecular electronics and magnetism.

Supplementary Materials: The following supporting information can be downloaded at: <https://www.mdpi.com/article/10.3390/nano12020224/s1>, Figure S1: Constant-height frequency shift nc-AFM images of the minority NGs formed on the Au(111) surface. Figure S2: Scheme of calculated PDOS of the different open-shell nonbenzenoid NGs labeling the position of the frontier orbitals SOMO, SUMO, HOMO and LUMO.

Author Contributions: J.I.U. and J.M. conceived the experiments. L.Y. synthesized and characterized the precursor under the supervision of J.M. and X.F. K.B., A.S.-G. and K.L. performed the STM, nc-AFM experiments and results interpretation. P.J. and Q.C. performed the theoretical calculations. J.I.U., D.É., R.M., J.M.G. and K.B. analyzed the data. All authors discussed the results and commented on the manuscript. All authors have read and agreed to the published version of the manuscript.

Funding: This project has received funding from Comunidad de Madrid [projects QUIMTRONIC-CM (Y2018/NMT-4783), MAD2D, and NanoMagCost], and Ministerio de Ciencia, Innovación y Universidades (projects SpOrQuMat, CTQ2017-83531-R, PID2019-108532GB-I00, and CTQ2016-81911-REDT). IMDEA Nanociencia is appreciative of support from the “Severo Ochoa” Programme for Centers of Excellence in R&D (MINECO, grant SEV-2016-0686). The EU Graphene Flagship (Graphene Core 3, 881603), H2020-EU.1.2.2.-FET Proactive Grant (LIGHT-CAP, 101017821), the Center for Advancing Electronics Dresden (cfaed) and the DFG-SNSF Joint Switzerland-German Research Project (EnhanTopo, No. 429265950) are acknowledged for financial support. We acknowledge support from the Praemium Academie of the Academy of Science of the Czech Republic and the CzechNanoLab Re-search Infrastructure supported by MEYS CR (LM2018110). P.J. acknowledges the support of the GACR 20-13692X. J.I.U. thanks the funding from the European Union’s Horizon 2020 research and innovation program under the Marie Skłodowska-Curie grant agreement No. [886314].

Institutional Review Board Statement: Not applicable.

Informed Consent Statement: Not applicable.

Data Availability Statement: The data presented in this study are available on request from the corresponding author.

Conflicts of Interest: The authors declare no conflict of interest.

References

1. Narita, A.; Wang, X.-Y.; Feng, X.; Müllen, K. New Advances in Nanographene Chemistry. *Chem. Soc. Rev.* **2015**, *44*, 6616–6643. [[CrossRef](#)]
2. Chen, L.; Hernandez, Y.; Feng, X.; Müllen, K. From Nanographene and Graphene Nanoribbons to Graphene Sheets: Chemical Synthesis. *Angew. Chem. Int. Ed.* **2012**, *51*, 7640–7654. [[CrossRef](#)]
3. Wu, J.; Pisula, W.; Müllen, K. Graphenes as Potential Material for Electronics. *Chem. Rev.* **2007**, *107*, 718–747. [[CrossRef](#)]
4. Zhi, L.; Müllen, K. A Bottom-up Approach from Molecular Nanographenes to Unconventional Carbon Materials. *J. Mater. Chem.* **2008**, *18*, 1472. [[CrossRef](#)]
5. Fujii, S.; Enoki, T. Nanographene and Graphene Edges: Electronic Structure and Nanofabrication. *Acc. Chem. Res.* **2013**, *46*, 2202–2210. [[CrossRef](#)]
6. Liu, J.; Feng, X. Synthetic Tailoring of Graphene Nanostructures with Zigzag-Edged Topologies: Progress and Perspectives. *Angew. Chem. Int. Ed.* **2020**, *59*, 23386–23401. [[CrossRef](#)]
7. Araujo, P.T.; Terrones, M.; Dresselhaus, M.S. Defects and Impurities in Graphene-like Materials. *Mater. Today* **2012**, *15*, 98–109. [[CrossRef](#)]
8. Sun, L.; Luo, Y.; Li, M.; Hu, G.; Xu, Y.; Tang, T.; Wen, J.; Li, X.; Wang, L. Role of Pyridinic-N for Nitrogen-Doped Graphene Quantum Dots in Oxygen Reaction Reduction. *J. Colloid Interface Sci.* **2017**, *508*, 154–158. [[CrossRef](#)]
9. Sun, Z.; Wu, J. Open-Shell Polycyclic Aromatic Hydrocarbons. *J. Mater. Chem.* **2012**, *22*, 4151–4160. [[CrossRef](#)]
10. Morita, Y.; Suzuki, S.; Sato, K.; Takui, T. Synthetic Organic Spin Chemistry for Structurally Well-Defined Open-Shell Graphene Fragments. *Nat. Chem.* **2011**, *3*, 197–204. [[CrossRef](#)]
11. Das, S.; Wu, J. Polycyclic Hydrocarbons with an Open-Shell Ground State. *Phys. Sci. Rev.* **2017**, *2*, 253–288. [[CrossRef](#)]
12. Gryn’ova, G.; Coote, M.L.; Corminboeuf, C. Theory and Practice of Uncommon Molecular Electronic Configurations. *WIREs Comput. Mol. Sci.* **2015**, *5*, 440–459. [[CrossRef](#)]
13. Shen, Q.; Gao, H.-Y.; Fuchs, H. Frontiers of On-Surface Synthesis: From Principles to Applications. *Nano Today* **2017**, *13*, 77–96. [[CrossRef](#)]

14. Urgel, J.I.; Hayashi, H.; Di Giovannantonio, M.; Pignedoli, C.A.; Mishra, S.; Deniz, O.; Yamashita, M.; Dienel, T.; Ruffieux, P.; Yamada, H.; et al. On-Surface Synthesis of Heptacene Organometallic Complexes. *J. Am. Chem. Soc.* **2017**, *139*, 11658–11661. [[CrossRef](#)]
15. Ayani, C.G.; Pizarra, M.; Urgel, J.I.; Jesús Navarro, J.; Díaz, C.; Hayashi, H.; Yamada, H.; Calleja, F.; Miranda, R.; Fasel, R.; et al. Efficient Photogeneration of Nonacene on Nanostructured Graphene. *Nanoscale Horiz.* **2021**, *6*, 744–750. [[CrossRef](#)]
16. Krüger, J.; García, F.; Eisenhut, F.; Skidin, D.; Alonso, J.M.; Guitián, E.; Pérez, D.; Cuniberti, G.; Moresco, F.; Peña, D. Decacene: On-Surface Generation. *Angew. Chem.* **2017**, *129*, 12107–12110. [[CrossRef](#)]
17. Zuzak, R.; Dorel, R.; Kolmer, M.; Szymonski, M.; Godlewski, S.; Echavarren, A.M. Higher Acenes by On-Surface Dehydrogenation: From Heptacene to Undecacene. *Angew. Chem. Int. Ed.* **2018**, *57*, 10500–10505. [[CrossRef](#)]
18. Eisenhut, F.; Kühne, T.; García, F.; Fernández, S.; Guitián, E.; Pérez, D.; Trinquier, G.; Cuniberti, G.; Joachim, C.; Peña, D.; et al. Dodecacene Generated on Surface: Reopening of the Energy Gap. *ACS Nano* **2020**, *14*, 1011–1017. [[CrossRef](#)]
19. Urgel, J.I.; Mishra, S.; Hayashi, H.; Wilhelm, J.; Pignedoli, C.A.; Giovannantonio, M.D.; Widmer, R.; Yamashita, M.; Hieda, N.; Ruffieux, P.; et al. On-Surface Light-Induced Generation of Higher Acenes and Elucidation of Their Open-Shell Character. *Nat. Commun.* **2019**, *10*, 861. [[CrossRef](#)]
20. Mishra, S.; Xu, K.; Eimre, K.; Komber, H.; Ma, J.; Pignedoli, C.A.; Fasel, R.; Feng, X.; Ruffieux, P. Synthesis and Characterization of [7] Triangulene. *Nanoscale* **2021**, *13*, 1624–1628. [[CrossRef](#)]
21. Su, J.; Telychko, M.; Song, S.; Lu, J. Triangulenes: From Precursor Design to On-Surface Synthesis and Characterization. *Angew. Chem. Int. Ed.* **2020**, *59*, 7658–7668. [[CrossRef](#)]
22. Xu, X.; Di Giovannantonio, M.; Urgel, J.I.; Pignedoli, C.A.; Ruffieux, P.; Müllen, K.; Fasel, R.; Narita, A. On-Surface Activation of Benzylic C-H Bonds for the Synthesis of Pentagon-Fused Graphene Nanoribbons. *Nano Res.* **2021**, *14*, 4754–4759. [[CrossRef](#)]
23. Mishra, S.; Lohr, T.G.; Pignedoli, C.A.; Liu, J.; Berger, R.; Urgel, J.I.; Müllen, K.; Feng, X.; Ruffieux, P.; Fasel, R. Tailoring Bond Topologies in Open-Shell Graphene Nanostructures. *ACS Nano* **2018**, *12*, 11917–11927. [[CrossRef](#)]
24. Lohr, T.G.; Urgel, J.I.; Eimre, K.; Liu, J.; Di Giovannantonio, M.; Mishra, S.; Berger, R.; Ruffieux, P.; Pignedoli, C.A.; Fasel, R.; et al. On-Surface Synthesis of Non-Benzenoid Nanographenes by Oxidative Ring-Closure and Ring-Rearrangement Reactions. *J. Am. Chem. Soc.* **2020**, *142*, 13565–13572. [[CrossRef](#)]
25. Di Giovannantonio, M.; Urgel, J.I.; Beser, U.; Yakutovich, A.V.; Wilhelm, J.; Pignedoli, C.A.; Ruffieux, P.; Narita, A.; Müllen, K.; Fasel, R. On-Surface Synthesis of Indenofluorene Polymers by Oxidative Five-Membered Ring Formation. *J. Am. Chem. Soc.* **2018**, *140*, 3532–3536. [[CrossRef](#)]
26. Di Giovannantonio, M.; Eimre, K.; Yakutovich, A.V.; Chen, Q.; Mishra, S.; Urgel, J.I.; Pignedoli, C.A.; Ruffieux, P.; Müllen, K.; Narita, A.; et al. On-Surface Synthesis of Antiaromatic and Open-Shell Indeno[2,1-b]fluorene Polymers and Their Lateral Fusion into Porous Ribbons. *J. Am. Chem. Soc.* **2019**, *141*, 12346–12354. [[CrossRef](#)]
27. Di Giovannantonio, M.; Chen, Q.; Urgel, J.I.; Ruffieux, P.; Pignedoli, C.A.; Müllen, K.; Narita, A.; Fasel, R. On-Surface Synthesis of Oligo(Indenoidene). *J. Am. Chem. Soc.* **2020**, *142*, 12925–12929. [[CrossRef](#)]
28. Mishra, S.; Beyer, D.; Eimre, K.; Kezilebieke, S.; Berger, R.; Gröning, O.; Pignedoli, C.A.; Müllen, K.; Liljeroth, P.; Ruffieux, P.; et al. Topological Frustration Induces Unconventional Magnetism in a Nanographene. *Nat. Nanotechnol.* **2020**, *15*, 22–28. [[CrossRef](#)]
29. Mishra, S.; Beyer, D.; Eimre, K.; Liu, J.; Berger, R.; Gröning, O.; Pignedoli, C.A.; Müllen, K.; Fasel, R.; Feng, X.; et al. Synthesis and Characterization of π -Extended Triangulene. *J. Am. Chem. Soc.* **2019**, *141*, 10621–10625. [[CrossRef](#)]
30. Mishra, S.; Beyer, D.; Berger, R.; Liu, J.; Gröning, O.; Urgel, J.I.; Müllen, K.; Ruffieux, P.; Feng, X.; Fasel, R. Topological Defect-Induced Magnetism in a Nanographene. *J. Am. Chem. Soc.* **2020**, *142*, 1147–1152. [[CrossRef](#)]
31. Mishra, S.; Beyer, D.; Eimre, K.; Ortiz, R.; Fernández-Rossier, J.; Berger, R.; Gröning, O.; Pignedoli, C.; Fasel, R.; Feng, X.; et al. Collective All-Carbon Magnetism in Triangulene Dimers. *Angew. Chem. Int. Ed.* **2020**, *59*, 12041–12047. [[CrossRef](#)]
32. Mishra, S.; Melidonie, J.; Eimre, K.; Obermann, S.; Gröning, O.; Pignedoli, C.A.; Ruffieux, P.; Feng, X.; Fasel, R. On-Surface Synthesis of Super-Heptazethrene. *Chem. Commun.* **2020**, *56*, 7467–7470. [[CrossRef](#)]
33. Mishra, S.; Yao, X.; Chen, Q.; Eimre, K.; Gröning, O.; Ortiz, R.; Di Giovannantonio, M.; Sancho-García, J.C.; Fernández-Rossier, J.; Pignedoli, C.A.; et al. Large Magnetic Exchange Coupling in Rhombus-Shaped Nanographenes with Zigzag Periphery. *Nat. Chem.* **2021**, *13*, 581–586. [[CrossRef](#)]
34. Gröning, O.; Wang, S.; Yao, X.; Pignedoli, C.A.; Borin Barin, G.; Daniels, C.; Cupo, A.; Meunier, V.; Feng, X.; Narita, A.; et al. Engineering of Robust Topological Quantum Phases in Graphene Nanoribbons. *Nature* **2018**, *560*, 209–213. [[CrossRef](#)]
35. Ruffieux, P.; Wang, S.; Yang, B.; Sánchez-Sánchez, C.; Liu, J.; Dienel, T.; Talirz, L.; Shinde, P.; Pignedoli, C.A.; Passerone, D.; et al. On-Surface Synthesis of Graphene Nanoribbons with Zigzag Edge Topology. *Nature* **2016**, *531*, 489–492. [[CrossRef](#)]
36. Li, J.; Sanz, S.; Castro-Esteban, J.; Vilas-Varela, M.; Friedrich, N.; Frederiksen, T.; Peña, D.; Pascual, J.I. Uncovering the Triplet Ground State of Triangular Graphene Nanoflakes Engineered with Atomic Precision on a Metal Surface. *Phys. Rev. Lett.* **2020**, *124*, 177201. [[CrossRef](#)]
37. Zheng, Y.; Li, C.; Xu, C.; Beyer, D.; Yue, X.; Zhao, Y.; Wang, G.; Guan, D.; Li, Y.; Zheng, H.; et al. Designer Spin Order in Diradical Nanographenes. *Nat. Commun.* **2020**, *11*, 6076. [[CrossRef](#)]
38. Giessibl, F.J. Atomic Resolution on Si(111)-(7 × 7) by Noncontact Atomic Force Microscopy with a Force Sensor Based on a Quartz Tuning Fork. *Appl. Phys. Lett.* **2000**, *76*, 1470–1472. [[CrossRef](#)]
39. Bartels, L.; Meyer, G.; Rieder, K.-H.; Velic, D.; Knoesel, E.; Hotzel, A.; Wolf, M.; Ertl, G. Dynamics of Electron-Induced Manipulation of Individual CO Molecules on Cu(111). *Phys. Rev. Lett.* **1998**, *80*, 2004–2007. [[CrossRef](#)]

40. Gross, L.; Mohn, F.; Moll, N.; Liljeroth, P.; Meyer, G. The Chemical Structure of a Molecule Resolved by Atomic Force Microscopy. *Science* **2009**, *325*, 1110–1114. [[CrossRef](#)]
41. Horcas, I.; Fernández, R.; Gómez-Rodríguez, J.M.; Colchero, J.; Gómez-Herrero, J.; Baro, A.M. WSXM: A Software for Scanning Probe Microscopy and a Tool for Nanotechnology. *Rev. Sci. Instrum.* **2007**, *78*, 013705. [[CrossRef](#)] [[PubMed](#)]
42. Zhao, Y.; Jiang, K.; Li, C.; Liu, Y.; Xu, C.; Zheng, W.; Guan, D.; Li, Y.; Zheng, H.; Liu, C.; et al. Precise Control of π -Electron Magnetism in Metal-Free Porphyrins. *J. Am. Chem. Soc.* **2020**, *142*, 18532–18540. [[CrossRef](#)] [[PubMed](#)]
43. Eisenhut, F.; Lehmann, T.; Viertel, A.; Skidin, D.; Krüger, J.; Nikipar, S.; Ryndyk, D.A.; Joachim, C.; Hecht, S.; Moresco, F.; et al. On-Surface Annulation Reaction Cascade for the Selective Synthesis of Diindenopyrene. *ACS Nano* **2017**, *11*, 12419–12425. [[CrossRef](#)] [[PubMed](#)]
44. Liu, J.; Mishra, S.; Pignedoli, C.A.; Passerone, D.; Urgel, J.I.; Fabrizio, A.; Lohr, T.G.; Ma, J.; Komber, H.; Baumgarten, M.; et al. Open-Shell Nonbenzenoid Nanographenes Containing Two Pairs of Pentagonal and Heptagonal Rings. *J. Am. Chem. Soc.* **2019**, *141*, 12011–12020. [[CrossRef](#)]
45. Mallada, B.; de la Torre, B.; Mendieta-Moreno, J.I.; Nachtigallová, D.; Matěj, A.; Matoušek, M.; Mutombo, P.; Brabec, J.; Veis, L.; Cadart, T.; et al. On-Surface Strain-Driven Synthesis of Nonalternant Non-Benzenoid Aromatic Compounds Containing Four- to Eight-Membered Rings. *J. Am. Chem. Soc.* **2021**, *143*, 14694–14702. [[CrossRef](#)] [[PubMed](#)]
46. Qiu, Z.; Sun, Q.; Wang, S.; Barin, G.B.; Dumslaff, B.; Ruffieux, P.; Müllen, K.; Narita, A.; Fasel, R. Exploring Intramolecular Methyl–Methyl Coupling on a Metal Surface for Edge-Extended Graphene Nanoribbons. *Org. Mater.* **2021**, *03*, 128–133. [[CrossRef](#)]
47. Hapala, P.; Kichin, G.; Wagner, C.; Tautz, F.S.; Temirov, R.; Jelínek, P. Mechanism of High-Resolution STM/AFM Imaging with Functionalized Tips. *Phys. Rev. B* **2014**, *90*, 085421. [[CrossRef](#)]
48. Goto, K.; Kubo, T.; Yamamoto, K.; Nakasuji, K.; Sato, K.; Shiomi, D.; Takui, T.; Kubota, M.; Kobayashi, T.; Yakusi, K.; et al. A Stable Neutral Hydrocarbon Radical: Synthesis, Crystal Structure, and Physical Properties of 2,5,8-Tri-Tert-Butyl-Phenalenyl. *J. Am. Chem. Soc.* **1999**, *121*, 1619–1620. [[CrossRef](#)]
49. Pavliček, N.; Mistry, A.; Majzik, Z.; Moll, N.; Meyer, G.; Fox, D.J.; Gross, L. Synthesis and Characterization of Triangulene. *Nat. Nanotechnol.* **2017**, *12*, 308–311. [[CrossRef](#)]
50. Su, J.; Telychko, M.; Hu, P.; Macam, G.; Mutombo, P.; Zhang, H.; Bao, Y.; Cheng, F.; Huang, Z.-Q.; Qiu, Z.; et al. Atomically Precise Bottom-up Synthesis of π -Extended [5] Triangulene. *Sci. Adv.* **2019**, *5*, eaav7717. [[CrossRef](#)]
51. Krejčí, O.; Hapala, P.; Ondráček, M.; Jelínek, P. Principles and Simulations of High-Resolution STM Imaging with a Flexible Tip Apex. *Phys. Rev. B* **2017**, *95*, 045407. [[CrossRef](#)]
52. Blum, V.; Gehrke, R.; Hanke, F.; Havu, P.; Havu, V.; Ren, X.; Reuter, K.; Scheffler, M. Ab Initio Molecular Simulations with Numeric Atom-Centered Orbitals. *Comput. Phys. Commun.* **2009**, *180*, 2175–2196. [[CrossRef](#)]
53. Becke, A.D. A New Mixing of Hartree–Fock and Local Density-functional Theories. *J. Chem. Phys.* **1993**, *98*, 1372–1377. [[CrossRef](#)]
54. Ternes, M.; Heinrich, A.J.; Schneider, W.-D. Spectroscopic Manifestations of the Kondo Effect on Single Adatoms. *J. Phys. Condens. Matter* **2008**, *21*, 053001. [[CrossRef](#)] [[PubMed](#)]
55. Ternes, M. Probing Magnetic Excitations and Correlations in Single and Coupled Spin Systems with Scanning Tunneling Spectroscopy. *Prog. Surf. Sci.* **2017**, *92*, 83–115. [[CrossRef](#)]
56. Sánchez-Grande, A.; Urgel, J.I.; Cahlik, A.; Santos, J.; Edalatmanesh, S.; Rodríguez-Sánchez, E.; Lauwaet, K.; Mutombo, P.; Nachtigallová, D.; Nieman, R.; et al. Diradical Organic One-Dimensional Polymers Synthesized on a Metallic Surface. *Angew. Chem. Int. Ed.* **2020**, *59*, 17594–17599. [[CrossRef](#)] [[PubMed](#)]